JRC Scientific and Technical Reports

# Envisat's Medium Resolution Imaging Spectrometer (MERIS)

## Algorithm Theoretical Basis Document:

## FAPAR and Rectified Channels over Terrestrial Surfaces

**Nadine Gobron**

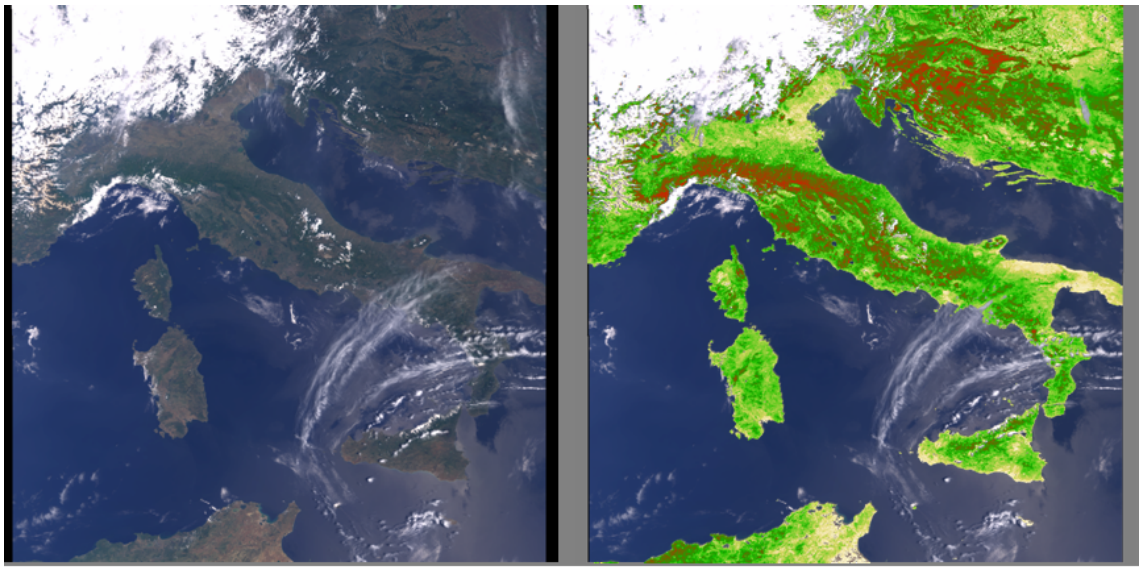

EUR 24844 EN

JRC EUROPEAN COMMISSION

ies Institute for Environment and Sustainability

The mission of the JRC-IES is to provide scientific-technical support to the European Union's policies for the protection and sustainable development of the European and global environment.

European Commission
Joint Research Centre
Institute for Environment and Sustainability

**Contact information**
Address: EC-JRC, TP 272, via E. Fermi, 2749. 21027 Ispra (VA) Italy
E-mail: nadine.gobron@jrc.ec.europa.eu
Tel.: +39 0332 786338
Fax: +39 0332 789073

`http://ies.jrc.ec.europa.eu`
`http://www.jrc.ec.europa.eu`



JRC65248

EUR 24844 EN
ISBN 978-92-79-20441-8
ISSN 1831-9424
doi:10.2788/27108

Luxembourg: Publications Office of the European Union



*Printed in Italy*

Contents

List of Figures

List of Tables

# 1. Introduction

## 1.1. Acronym and Abbreviations.

ATBd Algorithm Theoretical Basis document

BRF Bidirectional Reflectance Factor

ECV Essential Climate Variable

FAPAR Fraction of Absorbed Photosynthetically Active Radiation

GLI GLobal Imager

GTOS Global Terrestrial Observing System

GCOS Global Climate Observing System

JRC Joint Research Center

LUT Look Up Table

MERIS Medium Resolution Imaging Spectrometer

MODIS Moderate Resolution Imaging Spectroradiometer

MGVI MERIS Global Vegetation Index

OLCI Ocean Land Color Instrument

PAR Photosynthetic Active Radiation

RPV Rahman, Pinty, Verstraete

RT Radiative Transfer

SeaWiFS Sea-viewing Wide Field-of-view Sensor

TOA Top Of Atmosphere

TOC Top Of Canopy

1.2. **Purpose and Scope.** This Algorithm Theoretical Basis document (ATBd) describes the Joint Research Center (JRC)- procedure used to retrieve information of absorbed photosynthetical radiation by the vegetated terrestrial surfaces from an analysis of the Top Of Atmosphere (TOA) data acquired by Medium Resolution Imaging Spectrometer (MERIS) on board ENVISAT.

The code of the proposed algorithm takes the form of a set of several formulae which transform calibrated spectral directional reflectances into a single numerical value. These formulae are designed to extract the green Fraction of Absorbed Photosynthetically Active Radiation (FAPAR) in the plant canopy from the measurements and the rectified channels in the red and near-infrared bands.

The methodology described in this document has been optimized to assess the presence on the ground of healthy live green vegetation. The main optimization procedure has been constrained to provide an estimate of FAPAR in the plant canopy, although the outputs are expected to be used in a wide range of applications.

As example, such FAPAR data sets have been used into Carbon Cycle Data Assimilation (Kaminski et al. 2010; Knorr et al. 2010) or have been analysis for monitoring state of biosphere (Jung et al. 2010; Gobron et al. 2010). Regional data can also be served as a proxy for monitoring quasi near-real time the European drought (Rossi et al. 2010) or have been used for studying phenology (Richardson et al. 2010).

This algorithm delivers, in addition to the FAPAR product, the so-called rectified reflectance values in the red and near-infrared spectral bands. These are virtual reflectances largely decontaminated from atmospheric and angular effects. It also provides a categorization of pixel types thanks to a pre-processing

identification based on multi-spectral properties. These two virtual reflectances are also computed over bare soils using specific coefficients.

This document identifies the sources of input data, outlines the physical principles and mathematical background justifying this approach, describes the proposed algorithm, and lists the assumptions and limitations of this technique.

1.3. **Algorithm identification.** The algorithm described below is called the MERIS Global Vegetation Index (MGVI). It is suitable for any surface applications requiring the monitoring of the state of the land surface.

This document outlines the algorithm which is recommended to generate FAPAR product and associated rectifiedconstraints red and near-infrared reflectance values. Table 1 summarizes various versions of the ATBd.

A series of relevant reports and articles are included in the bibliography list.

Table 1. Document Change Record

| Version | Date | Description |
|---|---|---|
| 1.1 | 1999 | First Version - DPM |
| 2.0 | 2004 | Updated Formulae and Coefficients |
| 3.0 | 05/2011 | New products over bare soils Updated Identification of bare surfaces |

## 2. Algorithm overview

2.1. **Objectives.** The bulk of the solar radiation available to the Earth system is absorbed at or near the oceanic and continental surface. This energy is ultimately released to the atmosphere through the fluxes of infrared radiation, as well as sensible and latent heat. The phytosphere, which itself accounts for most of the biomass, affects these exchanges through a surface of contact (leaves) with the atmosphere estimated to be larger than the surface of the entire planet.

The state and evolution of terrestrial vegetation is characterized by a large number of physical, biochemical and physiological variables. Few of these are directly observable from space, but they jointly determine the FAPAR which acts as an integrated indicator of the status and health of the plant canopy, and can reasonably be retrieved by remote sensing techniques. FAPAR plays also a critical role in the biosphere path of the global carbon cycle and in the determination of the primary productivity of the phytosphere.

The properties of terrestrial surfaces thus concern a large number of users through such applications as agriculture, forestry, environmental monitoring, etc. Since plant canopies significantly affect the spectral and directional reflectance of solar radiation, it is expected that the analysis of repeated observations of these reflectances may lead to a better understanding of the fundamental processes controlling the biosphere, which, in turn, will support the definition of sustainable policies of environmental exploitation, and the control of the effectiveness of any adopted rules and regulations.

The FAPAR has been also recognized as one of the fundamental Essential Climate Variable (ECV) by Global Terrestrial Observing System (GTOS) and Global Climate Observing System (GCOS) (GCOS 2003).

A series of JRC-FAPAR algorithm has been optimized for various optical instrument such as SeaWiFS (Gobron et al. 2002), VEGETATION (Gobron et al. 2002b), GLobal Imager (GLI) (Gobron et al. 2002a) and Moderate Resolution Imaging Spectroradiometer (MODIS) (Gobron et al. 2006b) and (Gobron et al. 2006a).

Validation exercises for the FAPAR values at medium resolution scale have been performed for both Sea-viewing Wide Field-of-view Sensor (SeaWiFS) (Gobron et al. 2006) and MERIS (Gobron et al. 2008).

Such FAPAR algorithm is also proposed for the future Ocean Land Color Instrument (OLCI) (Gobron 2011) on board Sentinel-3 considering the continuity for having a long time series of observation requested for any global change applications.

The overall scientific objective of the JRC-FAPAR algorithm is to exploit the spectral reflectance measurements acquired by solar instruments to provide users with reliable qualitative and quantitative information on the state of the plant cover over terrestrial areas. Specifically, the output value is meant to be easily interpreted in terms of FAPAR values.

The design of the JRC-FAPAR requires, in a first step, the estimate of the so-called rectified reflectances at the red and near-infrared wavelengths in order to minimize atmospheric and angular perturbations. These intermediary land surface products should prove useful for documenting the state of the land surfaces and also assessing the spatio-temporal variations in land cover type.

We, therefore, also proposed in the reprocessing phase to compute these rectified channels over bare soils using specific training datasets corresponding to a variety of soils.

These rectified reflectances correspond to the amplitude parameter of the Bidirectional Reflectance Factor (BRF) entering the Rahman, Pinty, Verstraete (RPV) parametric model (Rahman et al. 1993).

These are virtual, *i.e.*, not directly measurable in the field, spectral reflectances which are, at best, decontaminated from atmospheric and angular effects.

2.2. **Instrument characteristics.** The MERIS instrument has been described in a number of publications, such as in Rast et al. (1999).

For the purpose of this document, it is sufficient to recall that MERIS is a programmable push-broom instrument acquiring multispectral measurements between 390 and 1040 nm, at a minimum usable resolution of 5 nm.

Fifteen bands of programmable location and width can be downloaded simultaneously at the full resolution at 300 m, at least for limited regions. Global coverage at a spatial resolution of 1.2 km are operationally available on a daily basis.

MERIS is not designed to acquire simultaneous measurements over any particular site under more than one geometry of illumination and observation. The proposed algorithm thus focus on the exploitation of the spectral variability of the data, keeping in mind the possible perturbing effects that may result from variations in geometry within and between successive images: A parametric anisotropic function is therefore implemented to account for such variations in the signal.

2.3. **Retrieval approach.** The specific objective of this document is to recall the algorithm suitable to estimate FAPAR optimized as already published in Gobron et al. (2004) which follows the same strategy used for a series of optical instrument such as SeaWiFS (Gobron et al. 2002), VEGETATION (Gobron et al. 2002b), GLobal Imager (GLI) (Gobron et al. 2002a), and MODIS (Gobron et al. 2006b; Gobron et al. 2006a).

The main criteria are:

(1) to provide a high sensitivity to the Fraction of Absorbed Photosynthetically Active Radiation (FAPAR) when a vegetated area is detected,

(2) to maintain a low sensitivity to soil and atmospheric conditions whenever vegetation is detected,

(3) to exploit the multi-band specificity of the sensor,

(4) to be independent of the geometry of illumination and observation, and

(5) to offer excellent discrimination capabilities, *i.e.*, the opportunity to distinguish various target types.

(6) to be independent of the spatial resolution.

## 3. Algorithm description

3.1. **Theoretical Description.** The general theory behind the design of optimal spectral indices has been described in Verstraete and Pinty (1996), and its specific application to medium resolution instruments has been addressed in Govaerts et al. (1999), Gobron et al. (1999) and Gobron et al. (2000).

The implementation of the algorithm assumes that, 1) the FAPAR can be used to quantify the presence of vegetation and, 2) radiation transfer model simulations can be used to define single appropriate scenarios over different representative land surfaces.

FAPAR estimates result from an analysis of multiple measurements with the help of a radiation transfer model in plant canopies using remote sensing observations as inputs.

"Total" FAPAR (absorbed component) is computed as the balance between sources and sinks, with positive inputs corresponding to:

- Incoming PAR at the top of the canopy (direct and/or diffuse);
- Incoming PAR from propagating horizontally (mostly important at very high spatial resolution) ;
- Light reflected by the underlying ground (soil and/or understory)

and losses corresponding to:

- Outgoing PAR reflected by the canopy (top and bottom)
- Outgoing PAR propagating horizontally

Leaves-only FAPAR refers to the fraction of PAR radiation absorbed by live leaves only, i.e., contributing to the photosynthetic activity within leaf cells.

This quantity is lower than "total" FAPAR because it does not include PAR absorption by the supporting woody material (in forest) or by dead leaves (in crops).

In particular, the retrieval method assumes that the leaves are alive and photosynthesizing, hence the name "green" FAPAR.

**We assume that the leaf single scattering albedo is 'fixed' to a value representing 'green' leaves using standard biochemical leaf properties.**

While FAPAR is typically based on an instantaneous measurement, for climate change applications representative daily values are required. They are obtained through direct measurements, or by assuming variation with the cosine of the solar zenith angle to obtain the daily leaves-only FAPAR.

The definition of FAPAR products as a balance of multiple fluxes remains dependent on the atmospheric conditions prevailing at the time of the measurements. In particular, estimates can be generated using direct, diffuse, or global radiation inputs. Knowledge on the type of incoming solar radiation fluxes is essential to properly interpret the data.

Similarly FAPAR can also be angularly integrated or instantaneous (i.e., at the actual sun position of measurement). As is the case for the surface albedo, one can define FAPAR estimates for a variety of atmospheric conditions and integrated in angles, space and times as needed.

**MGVI refers to the instantaneous and 'green' value definition.**

The bulk of the information on the presence of vegetation is contained *a priori* in the red and the near-infrared spectral bands, typically at wavelengths such as Band 8 and Band 14 of MERIS.

Addressing the atmospheric problem consists in converting Top Of Atmosphere (TOA) Bidirectional Reflectance Factors (BRFs) into Top Of Canopy (TOC) BRFs. Two classes of atmospheric radiative processes affect the measurements made by space-borne satellites: absorption and scattering. Absorption of radiation by specific gases can be largely avoided by carefully choosing the spectral location of narrow bands.

The effect of scattering cannot be avoided, and both molecular and aerosol scattering are strongly dependent on the wavelength of radiation. Hence, measurements in the blue region of the solar spectrum will provide values much more sensitive to atmospheric scattering than at longer wavelengths. In this approach, the characterization of plant canopies over fully or partially vegetated pixels currently relies on the analysis of data in 3 MERIS spectral bands, namely Band 2 at 442 $nm$, Band 8 at 681 $nm$, and Band 14 at 865 $nm$.

A Look Up Table (LUT) of bidirectional reflectance factors representing the MERIS like data is created using the physically-based semi-discrete model of Gobron et al. (1997) to represent the spectral and directional reflectance of horizontally homogeneous plant canopies, as well as to compute the values of FAPAR in each of them. The soil data required to specify the lower boundary condition in this model were taken from Price (1995).

In the case of bare soil, simulations is made with a modified Hapke model (Hapke 1981; Pinty et al. 1989) with a fixed hot-spot parameter equal to 0.2 and an asymmetry factor equal to -0.1. The value of single albedo, for each spectral bands, have been inverted to obtain the same albedo value as the lambertian assumption is made. The various geophysical scenarios performed to simulate the radiance fields are summarized in Table 3 and the geometrical conditions of illumination and observation are given in Table 4.

The spectral values for the leaf reflectance and transmittance were simulated using the leaf spectral model from Jacquemoud and Baret (1990) using standard leaf properties which correspond to the following biochemical values:

- Leaf internal structure parameter = 1.75,
- Leaf chlorophyll a+b content = 48.6 $\mu g cm^{-2}$,
- Leaf equivalent water thickness = 0.0115 $cm$,
- Leaf protein content = 0.00096 $gcm^{-2}$ and
- Leaf cellulose+lignin content = 0.00168 $gcm^{-2}$.

The Second Simulation of the Satellite Signal in the Solar Spectrum (6S) atmospheric model of Vermote et al. (1997) is used to represent the atmospheric absorption and scattering effects on the measured reflectances.

The FAPAR values are computed using the closure of the energy balance inside the plant canopy in the spectral range 400 to 700 nm. The various geophysical scenarios performed to simulate the radiance fields are summarized in Table 2 and the geometrical conditions of illumination and observation are given in Table 4. The sampling of the vegetation parameters and angular values were chosen to cover a wide range of environmental conditions. These simulations constitute the basic information used to optimize the formulae. The sampling selected to generate the Look Up Table (LUT) has been chosen so as to generate a robust global FAPAR algorithm.

Once this LUT is created, the design of the algorithm consists in defining the mathematical combination of spectral bands which best accounts for the variations of the variable of interest (here, FAPAR) on the basis of (simulated) measurements, while minimizing the effect of perturbing factors such as atmospheric or angular effects. This process is described in the next section.

All spectral simulations are done using specific spectral response of each band derived from MERIS instrument.

3.2. **Mathematical description of the algorithm.** The proposed algorithm to compute the FAPAR value, is organized around three main consecutive steps.

TABLE 2. Geophysical scenarios used to simulate the radiance fields over vegetation.

| **Medium** | **Variable** | **Meaning** | **Range of values** |
|---|---|---|---|
| Atmosphere model (Vermote *et al.*, 1997) | $\tau_s$ | Aerosol opt. thickness | .05, 0.3 and .8 |
| Vegetation model (Gobron *et al.*, 1997) | LAI | Leaf Area Index | 0, 0.5, 1, 2, 3, 4, and 5 |
| | $H_c$ | Height of Canopy | 0.5 m and 2 m |
| | $d_\ell$ | Equivalent diameter of single leaf | 0.01 m and 0.05 m |
| | LAD | Leaf Angle Distribution | Erectophile, Planophile |
| Soil data base (Price, 1995) | $r_s$ | Soil reflectance | 5 soil spectra, from dark to bright |

TABLE 3. Geophysical scenarios used to simulate the radiance fields over bare soils.

| **Medium** | **Variable** | **Meaning** | **Range of values** |
|---|---|---|---|
| Atmosphere model (Vermote *et al.*, 1997) | $\tau_s$ | Aerosol opt. thickness | .05, 0.3 and .8 |
| Vegetation model (Gobron *et al.*, 1997) | LAI | Leaf Area Index | 0 and 0.05 |
| | $H_c$ | Height of Canopy | 0.5 m and 2 m |
| | $d_\ell$ | Equivalent diameter of single leaf | 0.01 m and 0.05 m |
| | LAD | Leaf Angle Distribution | Erectophile, Planophile |
| Soil data base (Price, 1995) | $r_s$ | Soil reflectance | **7** soil spectra, from dark to very bright |
| Soil Model (Pinty et al., 1997) | $w_s$ | Single Scattering Albedo | from dark to bright |
| | $h_s$ | Hot-spot factor | 0.2 |
| | $\theta$ | Asymmetry Factor | -0.1 |

TABLE 4. Illumination and observation geometries used to simulate the radiance fields.

| **Variable** | **Angle** | **Values** |
|---|---|---|
| $\theta_0$ | Solar zenith angle | 20° and 50° |
| $\theta_v$ | Sensor zenith angle | 0°, 25° and 40° |
| $\phi$ | Sun-Sensor relative azimuth | 0°, 90° and 180° |

A As mentioned previously because of the sampling strategy that will be implemented by MERIS in the angular domain, it is not possible to retrieve the anisotropy of the radiance field. A parametric anisotropic function is implemented to account for variations in the signal due to changes in the geometrical conditions. The bidirectional reflectance model of Rahman et al. (1993) (RPV) is assumed to be appropriate for this task:

$$\rho_i(\theta_0, \theta_v, \phi) = \rho_{i0}\, F(\theta_0, \theta_v, \phi; k_i, \Theta_i^{hg}, \rho_{ic}) \tag{1}$$

where $F$ characterizes the anisotropy of the medium in terms of three unknown parameters, namely $k_i$, $\Theta_i^{hg}$ and $\rho_{ic}$ which depend exclusively on the intrinsic properties of the type of geophysical system for a given spectral band $i$. The function $F(\Omega; k_i, \Theta_i^{hg}, \rho_{ic})$ with $\Omega = (\theta_0, \theta_v, \phi)$ is given by:

$$F(\Omega; k_i, \Theta_i^{hg}, \rho_{ic}) = f_1(\theta_0, \theta_v, k_i)\, f_2(\Omega, \Theta_i^{hg})\, f_3(\Omega, \rho_{ic}) \tag{2}$$

where

$$f_1(\theta_0, \theta_v, k_i) = \frac{(\cos\theta_0 \cos\theta_v)^{k_i - 1}}{(\cos\theta_0 + \cos\theta_v)^{1-k_i}} \tag{3}$$

$$f_2(\Omega, \Theta_i^{hg}) = \frac{1 - \Theta_i^{hg\,2}}{\left(1 + 2\,\Theta_i^{hg}\,\cos g + \Theta_i^{hg\,2}\right)^{3/2}} \tag{4}$$

$$f_3(\Omega, \rho_{ic}) = 1 + \frac{1 - \rho_{ic}}{1 + G} \tag{5}$$

with

$$G = \left(\tan^2\theta_0 + \tan^2\theta_v - 2\,\tan\theta_0\,\tan\theta_v\,\cos\phi\right)^{1/2} \tag{6}$$

$$\cos g = \cos\theta_0\,\cos\theta_v + \sin\theta_0\,\sin\theta_v\cos\phi \tag{7}$$

The characterization of a geophysical system with the RPV model thus requires the estimation of four parameter values, namely $\rho_{i0}$, $k_i$, $\Theta_i^{hg}$ and, $\rho_{ic}$ which are independent of the geometry of illumination and observation $\Omega$.

The parameters intervening in function $F$ are optimized separately in the three bands using the simulated BRFs emerging at the top of atmosphere.

B The information contained in the band 2 (blue) is combined with that in the bands 8 and 14 (red and near-infrared) traditionally used to monitor vegetation, in order to generate "rectified bands" at these latter two wavelengths. The "rectification" is done in such a way as to minimize the difference between those rectified bands and the spectral reflectances that would have been measured at the top of the canopy under identical geometrical conditions but in the absence of the atmosphere.

C The FAPAR value is then generated on the basis of these "rectified bands".

The proposed algorithm assumes that ratios of polynomials are appropriate to generate both the "rectified bands" with the following generic formula:

$$g_n(x,y) = \frac{l_{n,1}(x + l_{n,2})^2 + l_{n,3}(y + l_{n,4})^2 + l_{n,5}xy}{l_{n,6}(x + l_{n,7})^2 + l_{n,8}(y + l_{n,9})^2 + l_{n,10}xy + l_{n,11}} \tag{8}$$

where $x$ and $y$ are the spectral bands at the appropriate step. The formula itself is given by the following formulae:

$$g_0(x,y) = \frac{l_{0,1}\,y - l_{0,2}\,x - l_{0,3}}{(l_{0,4} - x)^2 + (l_{0,5} - y)^2 + l_{0,6}} \tag{9}$$

$$\text{JRC-FAPAR} = g_0(\rho_{RBand8}, \rho_{RBand14}) \tag{10}$$

where $\rho_{Rred}$ and $\rho_{Rnir}$ are the rectified reflectance values in the red and near-infrared bands described above. These, in turn, are estimated with

$$\rho_{RBand8} = g_1(\tilde{\rho}_{Band2}, \tilde{\rho}_{Band8}) \tag{11}$$

$$\rho_{RBand14} = g_2(\tilde{\rho}_{Band2}, \tilde{\rho}_{Band14}) \tag{12}$$

where

$$\tilde{\rho}_i = \frac{\rho_i^*(\theta_0, \theta_v, \phi)}{F(\theta_0, \theta_v, \phi; k_i, \Theta_i^{hg}, \rho_{ic})} \tag{13}$$

and where $\rho_i^*$ denotes the (simulated) top of atmosphere bidirectional reflectance factor in band $i$, while $\tilde{\rho}_i$ is the bidirectional reflectance factor normalized by the anisotropic function $F$. An optimization procedure is applied to retrieve successively the optimal values of the coefficients intervening in the three steps mentioned above, namely $k_i$, $\Theta_i^{hg}$ and $\rho_{ic}$, and $l_{n,j}$ for the polynomials $g_n$, both for the rectified bands and for the final index itself.

A In the first step, it is assumed that the anisotropic shapes of the BRFs simulated at the top of the atmosphere may change with the spectral wavelength of interest, but do not depend on the geophysical systems specified to generate the BRFs. Accordingly, for a given spectral band, the three parameters of the anisotropic function $F$ are forced to be constant over each entire set of geophysical scenarios considered, *i.e.* vegetated or bare soil surface. In practice, this condition is achieved by minimizing the following cost functions:

$$\delta_i^2 = \sum_{\zeta,\Omega} \left[ \left( \frac{\rho_i^*(\Omega)}{F(\Omega; k_i, \Theta_i^{hg}, \rho_{ic})} \right) - \tilde{\rho}_i \right]^2 \rightarrow 0 \tag{14}$$

where $\zeta$ represents the geophysical domain and $\Omega$ the angular domain over which the optimization is sought.

Since $\tilde{\rho}_i$ is assumed to be constant in the RPV model for each individual geophysical system taken separately, we can estimate the mean value of the BRFs over the $\Omega$ space for every geophysical system:

$$\frac{1}{N_{obs}} \sum_{\Omega} \rho_i^*(\Omega_j) = \frac{1}{N_{obs}} \sum_{\Omega} \tilde{\rho}_i \times F(\Omega_j; k_i, \Theta_i^{hg}, \rho_{ic}) \tag{15}$$

$$= \tilde{\rho}_i \frac{1}{N_{obs}} \sum_{\Omega} F(\Omega_j; k_i, \Theta_i^{hg}, \rho_{ic}) \tag{16}$$

where $N_{obs}$ is the total number of angular situations. The model coefficient $\tilde{\rho}_i$ is thus approximated for each geophysical system as

$$\tilde{\rho}_i = \frac{1}{N_{obs}} \sum_{\Omega} \rho_i^*(\Omega_j) \Big/ \frac{1}{N_{obs}} \sum_{\Omega} F(\Omega_j; k_i, \Theta_i^{hg}, \rho_{ic}) \tag{17}$$

The cost function is rewritten as follows:

$$\delta_i^2 = \sum_{\zeta} \left[ \frac{\rho_i^*(\Omega)}{F(\Omega; k_i, \Theta_i^{hg}, \rho_{ic})} \frac{1}{N_{obs}} \sum_{\Omega} F(\Omega_j; k_i, \Theta_i^{hg}, \rho_{ic}) - \frac{1}{N_{obs}} \sum_{\Omega} \rho_i^*(\Omega_j) \right]^2 \rightarrow 0 \tag{18}$$

B To satisfy the various requirements described above, the optimization procedure is applied in the Band 8 and Band 14 separately, to derive the coefficients of $g_1$ and $g_2$. This is achieved by minimizing the following cost functions:

$$\delta_{g_i}^2 = \sum_{\zeta} \left[ g_i(\tilde{\rho}_{blue}, \tilde{\rho}_i) - \tilde{\rho}_i^{TOC} \right]^2 \rightarrow 0. \tag{19}$$

where

$$\tilde{\rho}_i^{TOC} = \frac{\rho_i^{TOC}(\Omega)}{F(\Omega, k_i^{TOC}, \Theta_i^{hg,TOC}, \rho_{ic}^{TOC})} \tag{20}$$

for which the anisotropic parameters, namely $k_i^{TOC}, \Theta_i^{hg,TOC}, \rho_{ic}^{TOC}$, were previously optimized at the top of canopy level.

C Following the rectification of the BRFs in the previous step, the coefficients of $g_0$ are evaluated by minimizing the following cost function:

$$\delta_{g_0}^2 = \sum_{\zeta} \left[ g_0(\rho_{Rred}, \rho_{Rnir}) - \mathrm{FAPAR}(\mu_0) \right]^2 \rightarrow 0. \tag{21}$$

In other words, output are forced to take on values as close as possible to the $FAPAR(\mu_0)$ associated with the specified plant canopy scenarios. The simulated top-of-atmosphere spectral and directional reflectances generated by the coupled model are exploited with an extended version of the FACOSI tool (Govaerts et al. 1999) to adjust the formulae on the basis of the given set of equations.

TABLE 5. Values of the parameters for the anisotropic function $F$.

| **band** | **Parameter values** | | |
|---|---|---|---|
| | $\rho_{ic}$ | $k_i$ | $\Theta_i^{hg}$ |
| Band 2 | 0.24012 | 0.56192 | −0.04203 |
| Band 8 | −0.46273 | 0.70879 | 0.03700 |
| Band 14 | 0.63841 | 0.86523 | −0.00123 |

TABLE 6. Coefficients for the polynomial $g_1$.

| $l_{1,1}$ | $l_{1,2}$ | $l_{1,3}$ | $l_{1,4}$ | $l_{1,5}$ | |
|---|---|---|---|---|---|
| −9.2615 | −0.029011 | 3.2545 | 0.055845 | 9.8268 | |
| $l_{1,6}$ | $l_{1,7}$ | $l_{1,8}$ | $l_{1,9}$ | $l_{1,10}$ | $l_{1,11}$ |
| 0 | 0 | 0 | 0 | 0 | 1.0 |

TABLE 7. Coefficients for the polynomial $g_2$.

| $l_{2,1}$ | $l_{2,2}$ | $l_{2,3}$ | $l_{2,4}$ | $l_{2,5}$ | |
|---|---|---|---|---|---|
| −0.47131 | −0.21018 | −0.045159 | 0.076505 | −0.80707 | |
| $l_{2,6}$ | $l_{2,7}$ | $l_{2,8}$ | $l_{2,9}$ | $l_{2,10}$ | $l_{2,11}$ |
| −0.048362 | −1.2471 | −0.54507 | −0.47602 | −1.1027 | 0.0 |

TABLE 8. Coefficients for the polynomial $g_0$.

| $l_{0,1}$ | $l_{0,2}$ | $l_{0,3}$ | $l_{0,4}$ | $l_{0,5}$ | $l_{0,6}$ |
|---|---|---|---|---|---|
| 0.255 | 0.306 | −0.0045 | −0.32 | 0.3 | −0.005 |

[a] Optimization using TOA & TOC vegetated and bare soil BRFs simulations.

3.3. **Results over vegetated pixels.** The numerical results are summarized in Tables 5 to 8.

Figures (1) and (2) illustrate the impact of the "rectification" procedure, which combines TOA reflectances in the Band 2 with TOA reflectances in the Bands 8 and 14, respectively. The left panels on these figures show the relationships between the spectral BRFs TOC normalized by the anisotropic function $F$, and BRFs TOA for all geophysical and angular scenarios described in Table 2 and Table 4. The scattering of the points is caused by changes in the atmospheric conditions and by the relative geometry of illumination and observation. The right panels show the effect of the "rectification" process, which reduces this dispersion. A perfect "rectification" would collapse all points on the 1:1 line for each of the surface types considered. It can be seen that this process is particularly efficient over dense vegetation, and that it reduces the systematic bias due to atmospheric effects on BRFs in both bands.

Figure (3) provides information on the performance of the algorithm in term of providing FAPAR values from the BRF TOA values. The right panel shows the isolines of the JRC-FAPAR values in the spectral space of the rectified bands in the red (x-axis) and near-infrared (y-axis). It can be seen that the values varies between 0 and 1 over partially and fully vegetated surfaces and takes negative values out of the spectral domain of interest. The left panel of the same figure shows that JRC-FAPAR output is close to the FAPAR with a root mean square deviation closed to 0.05. Most of the remaining variability is probably caused by the various conditions that were considered in the geophysical scenarios (see Table 2). In fact, this variability results from conflicting requirements on the insensitivity of the algorithm to soil, atmospheric and geometrical effects in the MERIS spectral bands.

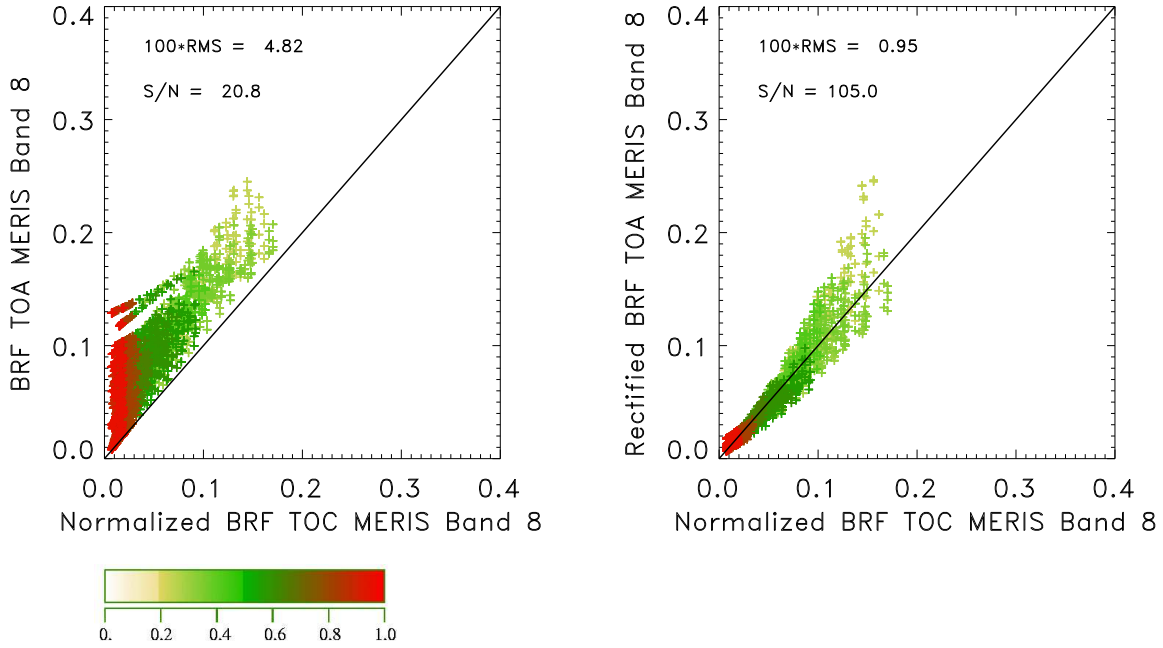


FIGURE 1. Left panel: relationship between the BRFs TOC normalized by the anisotropic function $F$, and BRFs TOA, for all conditions given in Table 2, in Band 8. Right panel: relationship between the "rectified" reflectances and the corresponding BRFs TOC normalized by the anisotropic function $F$. The various colours represent different values of FAPAR for the plant canopies described in Table 2.

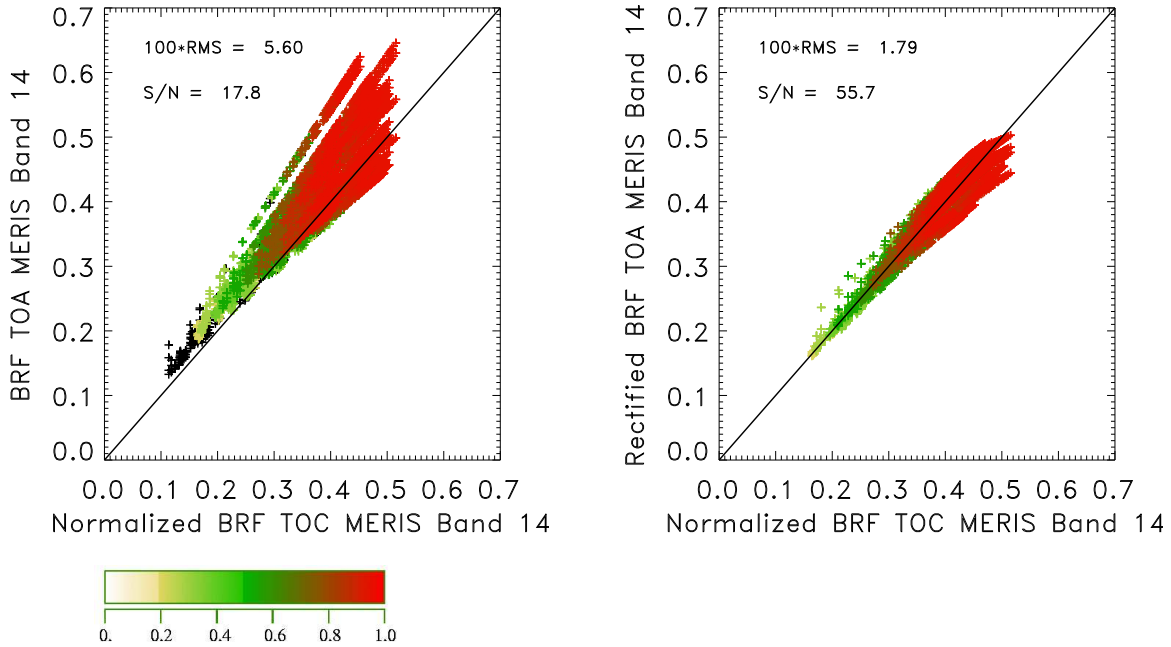


FIGURE 2. Same as Figure (1) except for Band 14.

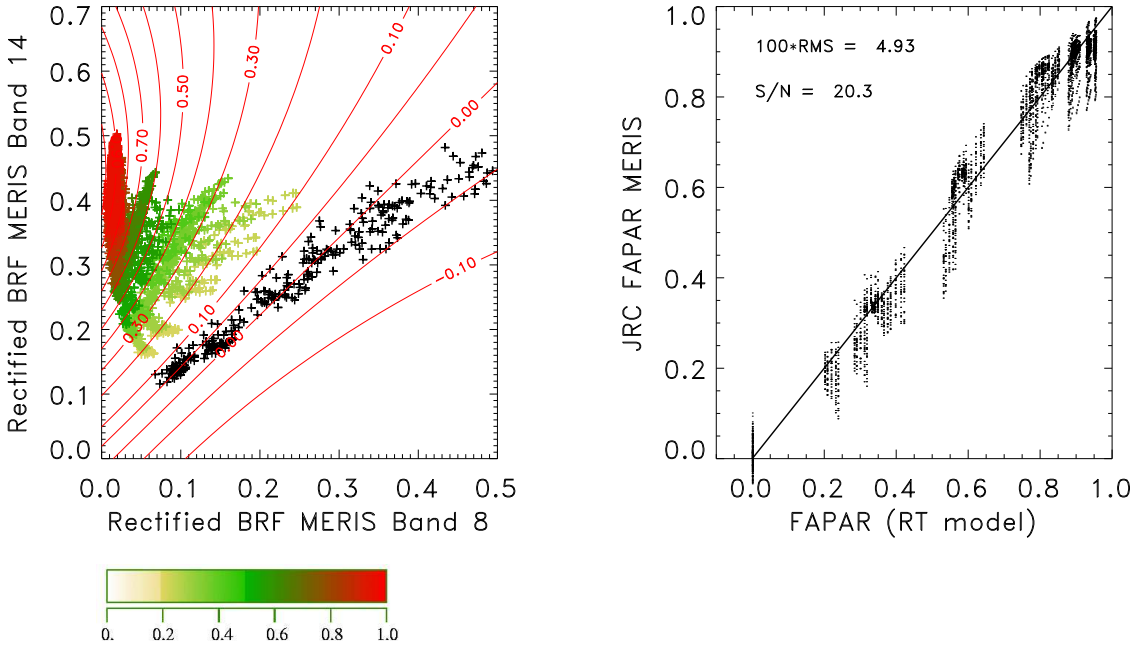


FIGURE 3. The left panel shows the isolines of JRC-FAPAR in the "rectified" spectral space together with the simulated radiances at the top of the atmosphere (see Table 2).The right panel shows the relationship between the index and the FAPAR values.

3.4. **Results over bare soils.** The numerical results are summarized in Tables 9 and 11.

TABLE 9. Values of the parameters for the anisotropic function $F$.

| **band** | **Parameter values** | | |
|---|---|---|---|
| | $\rho_{ic}$ | $k_i$ | $\Theta_i^{hg}$ |
| Band 2 | 0.42640 | 0.68545 | −0.02263 |
| Band 4 | 0.55649 | 0.87412 | −0.00357 |
| Band 14 | 0.65740 | 0.89788 | −0.01377 |

TABLE 10. Coefficients for the polynomial $g_1$.

| $l_{1,1}$ | $l_{1,2}$ | $l_{1,3}$ | $l_{1,4}$ | $l_{1,5}$ | |
|---|---|---|---|---|---|
| 0.79990 | 0.25117 | −0.24396 | 0.61913 | −1.7330 | |
| $l_{1,6}$ | $l_{1,7}$ | $l_{1,8}$ | $l_{1,9}$ | $l_{1,10}$ | $l_{1,11}$ |
| 6.3093 | 0.16104 | −0.10645 | −2.8388 | −9.1247 | 0.0 |

TABLE 11. Coefficients for the polynomial $g_2$.

| $l_{2,1}$ | $l_{2,2}$ | $l_{2,3}$ | $l_{2,4}$ | $l_{2,5}$ | |
|---|---|---|---|---|---|
| −0.10065 | −0.41872 | 0.12671 | −0.30530 | −0.39783 | |
| $l_{2,6}$ | $l_{2,7}$ | $l_{2,8}$ | $l_{2,9}$ | $l_{2,10}$ | $l_{2,11}$ |
| 0.56605 | 0.049710 | −0.11131 | −1.0396 | −0.87161 | |

Figures (4) and (5) illustrate the impact of the "rectification" procedure over bare soils, which combines TOA reflectances in the Band 2 with TOA reflectances in the Bands 8 and 14, respectively. The left panels on these figures show the relationships between the spectral BRFs TOC normalized by the anisotropic function $F$, and BRFs TOA for all geophysical and angular scenarios described in Table 3 and Table 4. The scattering of the points is caused by changes in the atmospheric conditions and by the relative geometry of illumination and observation. The right panels show the effect of the "rectification" process, which reduces this dispersion. A perfect "rectification" would collapse all points on the 1:1 line for each of the surface types considered.

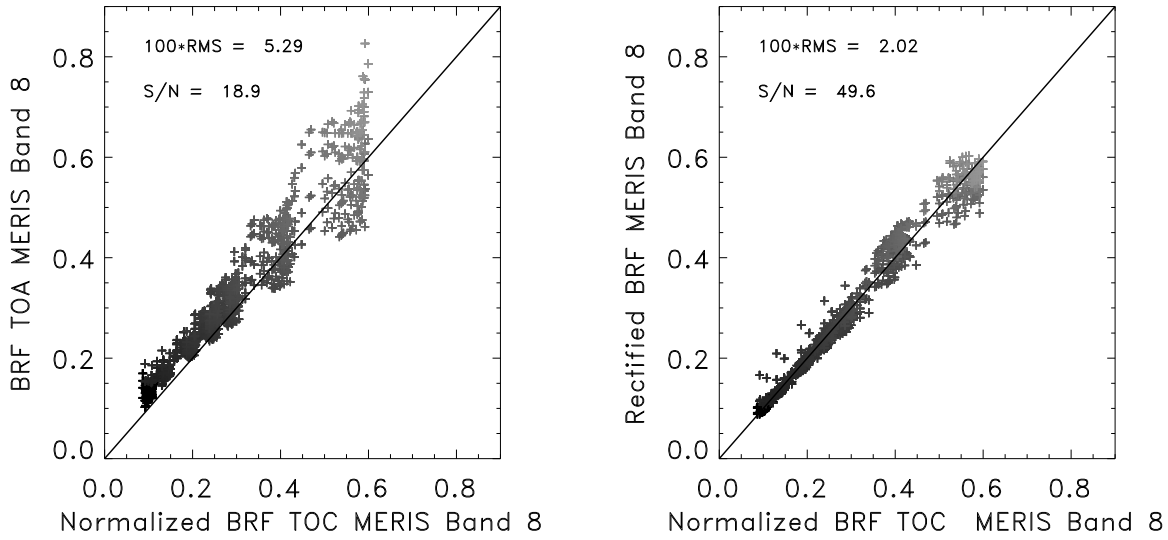


FIGURE 4. Left panel: relationship between the BRFs TOC normalized by the anisotropic function $F$, and BRFs TOA, for all conditions given in Table 3, in Band 8. Right panel: relationship between the "rectified" reflectances and the corresponding BRFs TOC normalized by the anisotropic function $F$.

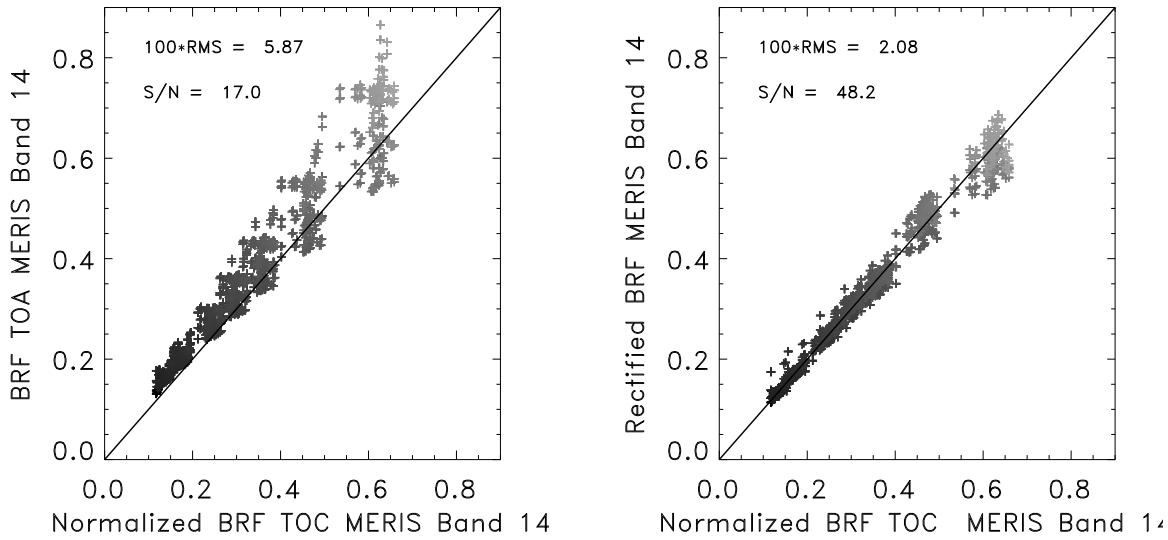


FIGURE 5. Same as Figure (4) except for Band 14.

## 4. Error budget estimates

Since the algorithm is optimized to provide a high sensitivity to FAPAR, a measurable biophysical variable, its capacity to detect the presence of green vegetation can be objectively assessed. For the particular geophysical scenarios in Table 2 and angular sampling given in Table 4, the root mean square deviation value of the fit between these two quantities is 0.05. Following the method proposed by Leprieur et al. (1994), the performance is evaluated with the help of a signal to noise ratio.

In the present case, it was found that the signal to noise ratio of the algorithm is equal to 20.3.

4.1. **Assessment of Uncertainties from TOA measurements.** The uncertainties of $g_i$ function can be first evaluated through a propagation error formulae:

$$(22) \quad |\Delta g_i(x_j)|^2 = \sum_{j=1}^{j=N} |\frac{\delta g_i(x_j)}{\delta(x_j)}|^2 \times |\Delta x_j|^2$$

were $x_j$ and $\Delta x_j$ are TOA BRFs and associated uncertainties in bands 2, 8 and 14, respectively.

The optimization of FAPAR algorithm gave a global theoretical accuracy between JRC-FAPAR and FAPAR simulated by RT model of 0.05 but this latter value can be evaluated on pixel value using the methodology described in the next section entitled "error estimates".

The total uncertainties of the algorithm for computed the FAPAR values can be therefore computed as the sum of the propagation error, $|\Delta g_0(x_i)|$, and the optimization error, $|\Delta FAPAR^{Opt}|$ :

$$(23) \quad |\Delta FAPAR| = |\Delta g_0(x_i)| + |\Delta FAPAR^{Opt}|$$

The associated uncertainties of the two rectified channels can be also computed such as:

$$(24) \quad |\Delta \rho_{R\lambda}| = |\Delta g_k(x_i)| + |\Delta \rho_{R\lambda}^{Opt}|$$

where $k = 1(2)$ when $\lambda$ =Band8 (Band14) respectively and $\Delta \rho_{R\lambda}^{Opt}$ are the uncertainties derived during the optimization processes. (Note that the latter values depend on pixels identification, *i.e.* vegetated or soil).

4.2. **Error estimates.**

4.2.1. *Radiative Transfer Models.* The FAPAR algorithm is based on radiative transfer theory through four radiative transfer models, *i.e.* the semi-discrete for vegetated canopies (Gobron et al. 1997, ), the Hapke modified soil model (Pinty et al. 1989, ), the 6S model for the atmosphere (Vermote et al. 1997, ) and the RPV parametric model (Rahman et al. 1993) for removing angular effects. Using these RT models imply the use of assumptions which can be taken into account for error estimates. Review on scientific literature assess the quality of these models which have been already benchmarked during international inter-comparisons (`http://rami-benchmark.jrc.ec.europa.eu`).

4.2.2. *Topographic effects.* Previous studies by Combal et al. (2000) on the effect of topographic variations on top of canopy reflectance values in the red and near-infrared bands shows that BRF TOC may differ from that of horizontal terrain from less than 5 % when the sun zenith angle is less than 40° . A maximum value is 10% occurs when the sun zenith angle is 60° at forward scattering directions for slopes of 10° or less. These differences depend on leaf area index values but are in the same directions in the red and near-infrared bands (see figure 3 of Combal et al. (2000)).

4.2.3. *FAPAR definition.* As it has been mentioned in previous section 3.1, this algorithm computes the instantaneous FAPAR for 'green' leaf under direct incoming radiation. The error due to this assumption against other type of FAPAR definition can be part of errors estimates.

### 4.3. **Practical consideration.**

4.3.1. *Quality control and diagnostics.* A simple approach is proposed to associate a label to each pixel of the MERIS data in order to optimize the various steps of the processing to be achieved over terrestrial surfaces.

Table 12 indicates the tests applied and the associated categories for discriminating the major geophysical systems (also identified with an identification number), namely clouds, bright surfaces, vegetated surfaces and water bodies. In the data product, the various identification numbers correspond to a set of flag values.

As can be seen from Table 12, the pixel labeling is performed on the basis of an ensemble of thresholds using only the values in the spectral bands used in the algorithm. For each geophysical category, the ensemble of tests has been established on the basis of knowledge of the multi-spectral signatures of the geophysical systems. The proposed approach classifies the vast majority of the pixels without requiring any other ancillary information. A more sophisticated labeling scheme could not be reasonably considered given the processing constraints imposed by the computing resources. However, other mask made in other MERIS products definition package can be added to the top of this one, such as the cloud detection one.

4.3.2. *Output.* The output generated by this algorithm consists in one FAPAR value, one value for the rectified red and near-infrared plus their own uncertainties, respectively.

The output field also contains the description of the geometry of illumination and observation, and one flag value for each pixel in the data input stream.

The flag value corresponds to the identification (ID) numbers described in section 4.3.1.

If the ID value is equal to 0, the value of FAPAR and rectified values are considered valid and the physical range of values lies in between 0 and 1.0.

If the ID number is equal either to 1 (“bad data”), 2 (“cloud, snow and ice”) or 3 (“water body and deep shadow”), the value of FAPAR and rectified values have not been computed and the reported values are equal to its error value.

If the ID number is equal to 4 (“bright surface”), the value of FAPAR has been set at 0 and rectified values are considered valid and the physical range of values lies in between 0 and 1.0.

If ID number is equal to 5 (“undefined”), the reported values are set to its error value.

If the ID number is equal to 6, the value was less than 0 and the reported value is equal to its error value.

If the ID number is equal to 7, the value was larger than 1 and the reported value is reset to 1 for the FAPAR.

## 5. Assumptions and limitations

5.1. **Assumptions.** The following assumptions have been made in the design of the MGVI :

(1) The spectral reflectances used as input to this algorithm have to be corrected for the seasonally variable distance between the Earth and the Sun.

(2) The plane-parallel approximation for radiation transfer has been assumed to be valid in the atmosphere.

(3) Plant canopies are assumed to be horizontally homogeneous within the MERIS pixel.

(4) All orographic effects have been ignored.

(5) Adjacency effects have been ignored.

TABLE 12. Pixel labeling criteria

| Identification number (ID) | Spectral tests | Associated categories |
|---|---|---|
| 0 | $0 < \rho_{Band2} < 0.3$ and $0 < \rho_{Band8} < 0.5$ and $0 < \rho_{Band14} < 0.7$ and $0 < \rho_{Band2} \leq \rho_{Band14}$ and $\rho_{Band14} \geq \mathbf{1.3}\,\rho_{Band8}$ | Vegetated surface |
| 1 | $\rho_{Band2} \leq 0$ or $\rho_{Band8} \leq 0$ or $\rho_{Band14} \leq 0$ | bad data |
| 2 | $\rho_{Band2} \geq 0.3$ or $\rho_{Band8} \geq 0.5$ or $\rho_{Band14} \geq 0.7$ | cloud, snow and ice |
| 3 | $0 < \rho_{Band2} < 0.3$ and $0 < \rho_{Band8} < 0.5$ and $0 < \rho_{Band14} < 0.7$ and $\rho_{Band2} > \rho_{Band14}$ | water body and deep shadow |
| 4 | $0 < \rho_{Band2} < 0.3$ and $0 < \rho_{Band8} < 0.5$ and $0 < \rho_{Band14} < 0.7$ and $0 < \rho_{Band2} \leq \rho_{Band14}$ and $\mathbf{1.3}\,\rho_{Band8} > \rho_{Band14}$ | Bright surface |
| 5 | $\rho_{R_{Band8}} < 0$ or $\rho_{R_{Band14}} < 0$ | undefined |
| 6 | $FAPAR < 0$ | no vegetation |
| 7 | $FAPAR > 1$ | vegetation (out of bounds) |

5.2. **Limitations.** The following limitations apply to the algorithm described in this version of the document:

(1) The retrieval of vegetation characteristics in hilly or mountainous regions may or may not be reliable. If the approach turns out to be unreliable in the presence of significant topographical features, additional tests may have to be implemented to screen out these regions on the basis of appropriate Digital Elevation Model (DEM) data. This would imply access to the corresponding elevation data sets, to reliably navigated MERIS data, and the presence of an additional orographic flag.

(2) The optimization of the algorithm was performed using a set of simulated TOA reflectance values which are expected to represent the most commonly encountered geophysical conditions. Although a wide range of possibilities were investigated, there is no guarantee that the most common geophysical scenarios have been implemented.

(3) The sun zenith angle should be lower than 60° (due to the limitation of the radiative transfer models.)

(4) The viewing zenith angle should be smaller than 40° .

# 6. Requirements

The implementation of the proposed algorithm to estimate FAPAR and rectified channels requires three different types of information, namely, the input data from the MERIS sensor, a set of ancillary data and a set of mathematical functions (Equations 8 to 13). The ancillary data are the set of coefficients given in Tables 5 to 8 over vegetated surfaces and in Tables 9 to 11 over bare soil surfaces.

The input data are the BRFs measured by the instrument at Band 2, Band 8 and band 14, together with the geometrical conditions of illumination and observation, namely $\theta_0, \theta_v, \phi$. The sun-sensor relative azimuth, $\phi$, is limited to the range [0°, 180°] and the backscatter/hot spot (forwardscatter/specular) direction is defined at 0° (180°).

## References

Combal, B., H. Isaka, and C. Trotter (2000). Extending a turbid medium BRDF model to allow sloping terrain with a vertical plant stand. *Geoscience and Remote Sensing, IEEE Transactions on 38*(2), 798 –810.

GCOS (2003). Summary Report of the eleventh session of the WMO-IOC-UNEP-ICSU (WMO/TD-No.1189). Report Melbourne, Australia, April 7-10 GCOS-87, World Meteorological Organization.

Gobron, N. (2011). Ocean and Land Colour Instrument (OLCI) FAPAR and Rectied Channels over Terrestrial Surfaces Algorithm Theoretical Basis Document . EUR Report No. xxxxx EN, Institute for Environment and Sustainability.

Gobron, N., O. Aussedat, and B. Pinty (2006a). MODerate resolution Imaging Spectroradiometer (MODIS) - JRC-FAPAR at 250m Algorithm Theoretical Basis Document. EUR Report 22279 EN, European Commission - DG Joint Research Centre, Institute for Environment and Sustainability.

Gobron, N., O. Aussedat, and B. Pinty (2006b). MODerate Resolution Imaging Spectroradiometer (MODIS), JRC-FAPAR Algorithm Theoretical Basis Document. EUR Report No. 22164 EN, Institute for Environment and Sustainability.

Gobron, N., O. Aussedat, B. Pinty, M. Taberner, and M. M. Verstraete (2004). Medium Resolution Imaging Spectrometer (MERIS) - Level 2 Land Surface Products - Algorithm Theoretical Basis Document-Revision 3.0. EUR Report No. 21387 EN, Institute for Environment and Sustainability.

Gobron, N., A. S. Belward, B. Pinty, and W. Knorr (2010). Monitoring biosphere vegetation 1998-2009. *Geophysical Research Letters 37*, L15402.

Gobron, N., B. Pinty, O. Aussedat, J. M. Chen, W. B. Cohen, R. Fensholt, V. Gond, K. F. Huemmrich, T. Lavergne, F. Mlin, J. L. Privette, I. Sandholt, M. Taberner, D. P. Turner, M. Verstraete, and J.-l. Widlowski (2006). Evaluation of FAPAR Products for Different Canopy Radiation Transfer Regimes: Methodology and Results using JRC Products Derived from SeaWiFS against ground-based estimations. *Journal of Geophysical Research 111*.

Gobron, N., B. Pinty, O. Aussedat, M. Taberner, O. Faber, F. Mélin, T. Lavergne, M. Robustelli, and P. Snoeij (2008). Uncertainty estimates for the FAPAR operational products derived from MERIS - Impact of top-of-atmosphere radiance uncertainties and validation with field data. *Remote Sensing of Environment 112*, 18711883.

Gobron, N., B. Pinty, F. Mélin, M. Taberner, and M. M. Verstraete (2002). Sea Wide Field-of-View Sensor (SeaWiFS) - An optimized FAPAR algorithm - Theoretical Basis Document. EUR Report No. 20148 EN, Institute for Environment and Sustainability.

Gobron, N., B. Pinty, M. M. Verstraete, and Y. Govaerts (1997). A semi-discrete model for the scattering of light by vegetation. *Journal of Geophysical Research 102*, 9431–9446.

Gobron, N., B. Pinty, M. M. Verstraete, and Y. Govaerts (1999). The MERIS Global Vegetation Index (MGVI): description and preliminary application. *International Journal of Remote Sensing 20*, 1917–1927.

Gobron, N., B. Pinty, M. M. Verstraete, and M. Taberner (2002a). Global Land Imager (GLI) - An optimized FAPAR algorithm - Theoretical Basis Document. EUR Report No. 20147 EN, Institute for Environment and Sustainability.

Gobron, N., B. Pinty, M. M. Verstraete, and M. Taberner (2002b). VEGETATION - An optimized FAPAR algorithm - Theoretical Basis Document. EUR Report No. 20146 EN, Institute for Environment and Sustainability.

Gobron, N., B. Pinty, M. M. Verstraete, and J.-L. Widlowski (2000). Advanced spectral algorithm and new vegetation indices optimized for up coming sensors: Development, accuracy and applications. *IEEE Transactions on Geoscience and Remote Sensing 38*, 2489–2505.

Govaerts, Y., M. M. Verstraete, B. Pinty, and N. Gobron (1999). Designing optimal spectral indices: a feasibility and proof of concept study. *International Journal of Remote Sensing 20*, 1853–1873.

Hapke, B. (1981). Bidirectional reflectance spectroscopy. I. Theory. *Journal of Geophysical Research 86*, 3039–3054.

Jacquemoud, S. and F. Baret (1990). PROSPECT: A model of leaf optical properties spectra. *Remote Sensing of Environment 34*, 75–91.

Jung, M., M. Reichstein, P. Ciais, S. I. Seneviratne, J. Sheffield, G. Bonan, A. Cescatti, J. Chen, R. A. M. de Jeu, A. J. H. Dolman, W. Eugster, D. Gerten, D. Gianelle, N. Gobron, et al. (2010).

Recent decline in the global land evapotranspiration trend due to limited moisture supply. *Nature 467*(7318), 951–954.

Kaminski, T., W. Knorr, M. Scholze, N. Gobron, B. Pinty, and P.-P. Mathieu (2010). Assimilation of meris fapar into a terrestrial vegetation model and mission design. In *2010 ESA Living Planet Symposium. Bergen, Norway, 28 June 2010 - 2 July 2010*, Volume 686 of *ESA Special Publication*. European Space Agency.

Knorr, W., T. Kaminski, M. Scholze, N. Gobron, B. Pinty, R. Giering, and P.-P. Mathieu (2010). Carbon cycle data assimilation with a generic phenology model. *Journal of Geophysical Research Biogeosciences 115*(9), G04017.

Leprieur, C., M. M. Verstraete, and B. Pinty (1994). Evaluation of the performance of various vegetation indices to retrieve vegetation cover from AVHRR data. *Remote Sensing Reviews 10*, 265–284.

Pinty, B., M. M. Verstraete, and R. E. Dickinson (1989). A physical model for predicting bidirectional reflectances over bare soil. *Remote Sensing of Environment 27*, 273–288.

Price, J. C. (1995). Examples of high resolution visible to near-infrared reflectance spectra and a standardized collection for remote sensing studies. *International Journal of Remote Sensing 16*, 993–1000.

Rahman, H., B. Pinty, and M. M. Verstraete (1993). Coupled surface-atmosphere reflectance (CSAR) model. 2. Semiempirical surface model usable with NOAA Advanced Very High Resolution Radiometer data. *Journal of Geophysical Research 98*, 20,791–20,801.

Rast, M., J.-L. Bézy, and S. Bruzzi (1999). The ESA Medium Resolution Imaging Spectrometer MERIS -a review of the instrument and its mission. *International Journal of Remote Sensing 20*, (1682–1701).

Richardson, A. J., T. A. Black, P. Ciais, N. Delbart, M. A. Friedl, N. Gobron, D. Y. Hollinger, et al. (2010). Influence of spring and autumn phenological transitions on forest ecosystem productivity. *Philosophical Transactions of the Royal Society B. Special issue on The Role of Phenology in Ecology and Evolution 365*(1555), 3227–3246.

Rossi, S., S. Niemeyer, and N. Gobron (2010). Meris fapar as a drought indicator: performance in different contexts. In *2010 ESA Living Planet Symposium. Bergen, Norway, 28 June 2010 - 2 July 2010*, Volume 686 of *ESA Special Publication*. European Space Agency.

Vermote, E., D. Tanré, J. L. Deuzé, M. Herman, and J. J. Morcrette (1997). Second simulation of the satellite signal in the solar spectrum: An overview. *IEEE Trans. Geoscience Remote Sensing 35-3*, 675–686.

Verstraete, M. M. and B. Pinty (1996). Designing optimal spectral indices for remote sensing applications. *IEEE Transactions on Geoscience and Remote Sensing 34*, 1254–1265.

European Commission

**EUR 24844 EN - Joint Research Centre - Institute for Environment and Sustainability**
Title: Envisat's Medium Resolution Imaging Spectrometer (MERIS) Algorithm Theoretical Basis Document: FAPAR and Rectified Channels over Terrestrial Surfaces.
Author: Nadine Gobron
Luxembourg: Publications Office of the European Union
2011 - 27 pp. - 21 × 29,7 cm
EUR - Scientific and Technical Research series - ISSN 1018-5593 (print), ISSN 1831-9424 (online)

ISBN 978-92-79-20441-8
doi:10.2788/27108

**Abstract**

This Algorithm Theoretical Basis document (ATBd) describes the Joint Research Center (JRC)- procedure used to retrieve information of absorbed photosynthetical radiation by the vegetated terrestrial surfaces from an analysis of the Top Of Atmosphere (TOA) data acquired by MERIS.

The code of the proposed algorithm takes the form of a set of several formulae which transform calibrated spectral directional reflectances into a single numerical value. These formulae are designed to extract the green Fraction of Absorbed Photosynthetically Active Radiation (FAPAR) in the plant canopy from the measurements and the rectified channels in the red and near-infrared bands.

The methodology described in this document has been optimized to assess the presence on the ground of healthy live green vegetation. The main optimization procedure has been constrained to provide an estimate of FAPAR in the plant canopy, although the outputs are expected to be used in a wide range of applications.

This algorithm delivers, in addition to the FAPAR product, the so-called rectified reflectance values in the red and near-infrared spectral bands. These are virtual reflectances largely decontaminated from atmospheric and angular effects. It also provides a categorization of pixel types thanks to a pre-processing identification based on multi-spectral properties. These two virtual reflectances are also computed over bare soils using specific coefficients.

This document identifies the sources of input data, outlines the physical principles and mathematical background justifying this approach, describes the proposed algorithm, and lists the assumptions and limitations of this technique.

**How to obtain EU publications**

Our priced publications are available from EU Bookshop (http://bookshop.europa.eu), where you can place an order with the sales agent of your choice.

The Publications Office has a worldwide network of sales agents. You can obtain their contact details by sending a fax to (352) 29 29-42758.

The mission of the JRC is to provide customer-driven scientific and technical support for the conception, development, implementation and monitoring of EU policies. As a service of the European Commission, the JRC functions as a reference centre of science and technology for the Union. Close to the policy-making process, it serves the common interest of the Member States, while being independent of special interests, whether private or national.


LB-NA-24844-EN-N


ISBN 978-92-79-20441-8